Thermoelectric effects and magnetic anisotropy of $Ga_{1-x}Mn_xAs$ thin films

I. V. Soldatov,[1,2,3,*] N. Panarina,[4] C. Hess,[4,5] L. Schultz,[1,2] and R. Schäfer[1,2]

[1]*Institute for Metallic Materials, Leibniz Institute for Solid State and Materials Research, IFW Dresden, Helmholtzstrasse 20, 01069 Dresden, Germany*

[2]*Institute for Materials Science, TU Dresden, 01062 Dresden, Germany*

[3]*Institute of Natural Sciences, Ural Federal University, 620000 Ekaterinburg, Russia*

[4]*Institute for Solid State Research, Leibniz Institute for Solid State and Materials Research, IFW Dresden, Helmholtzstrasse 20, 01069 Dresden, Germany*

[5]*Center for Transport and Devices, TU Dresden, 01069 Dresden, Germany*

(Received 18 June 2014; revised manuscript received 2 September 2014; published 24 September 2014)

The transverse voltages generated in a $Ga_{1-x}Mn_xAs$ ferromagnetic semiconductor in planar Hall effect and transverse spin Seebeck effect configurations are systematically analyzed. The observed field dependences consist of symmetric and asymmetric contributions. The former is attributed to the planar Nernst effect in the magnetic film in the presence of an in-plane temperature gradient, while the latter is caused by the anomalous Nernst effect due to spurious out-of-plane temperature gradients with a coefficient as high as 500 μV/K. We also report on the experimental observation of the planar Hall effect measured at different temperatures. Using a Stoner-Wohlfarth model for data analysis, the anisotropy constants K_u and K_c of superimposed uniaxial and cubic anisotropies in the magnetic film are determined. The temperature dependence of the K_u/K_c ratio reveals a gradual substitution of the cubic anisotropy dominating at low temperatures with the uniaxial anisotropy as the temperature rises. This behavior is confirmed by the simultaneous domain observation using Kerr microscopy, demonstrating different field evolutions of the domain structure at different temperatures.

DOI: 10.1103/PhysRevB.90.104423 PACS number(s): 72.25.−b, 72.20.Pa, 75.50.Pp, 85.75.−d

I. INTRODUCTION

A rapid pace of technological development causes the miniaturization of logic elements and encourages the search for an alternative to charge-flow-based electronic devices in order to increase the efficiency and to reduce Joule heating. Prominent candidates for new-generation electronics are spin-flow-based devices, which have attracted much attention recently. The efforts to generate and manipulate a spin flow gave rise to a new field of research called "spin caloritronics," in which the interaction of charge and spin degrees of freedom is exploited. From that perspective, magnetic semiconductors are very intriguing materials, as the spin-caloritronic phenomena measured on such structures are enhanced due to the strong spin-orbit coupling. Recently a number of effects have been reported in magnetic semiconducting thin films of $Ga_{1-x}Mn_xAs$: (i) the planar Nernst effect (PNE; a transverse thermopower generated by thermal gradients applied in the plane of the film) [1]; (ii) the anomalous Nernst effect (ANE; the occurrence of a spin-dependent transverse electric field in the presence of a temperature gradient)[2]; and (iii) the recently discovered spin Seebeck effect (SSE; the generation of spin currents by temperature gradients) [1,3,4]. The experimental configurations for measurement of these thermoelectric effects are schematically summarized in Figs. 1(b)–1(d).

Despite the rapid advancement of recent experimental [3,5–7] and theoretical studies [8,9] in thermoelectricity and magnetoelectronics, spin-dependent transport remains poorly understood. One of the possible routes to shed light on the underlying physics is to perform an accurate experiment in which all possible origins of ordinary and spin-related

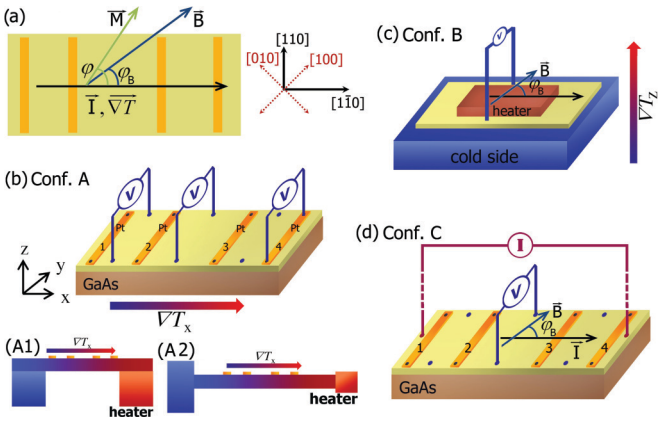

FIG. 1. (Color online) (a) Sample geometry and orientation of crystallographic axes. (b) Configuration A. Two variations of the scheme used for SSE and PNE measurements: (1) sample on top of the copper blocks and (2) face-to-face geometry. (c) Configuration B: geometry of ANE measurements. (d) Configuration C: geometry of PHE measurements at a constant temperature.

thermoelectric effects are taken into account. At present it is considered that the purest SSE is observed on insulators/metal interfaces, e.g., yttrium-iron-garnet (YIG)/Pt structures [10], as spurious contributions from ordinary thermoelectric effects in such systems without mobile charge carriers can be *a priori* neglected. However, the role of a proximity effect at the interface between platinum (which is used to measure the SSE via the inverse spin Hall effect) and a ferromagnetic insulator [11,12] remains an open question and demands proper consideration as well. As ordinary thermoelectric effects are highly dependent on the magnetization vector orientation, detailed knowledge of the magnetic anisotropy of the sample

*inmaze@mail.ru

is of great importance. In the present study we have combined twoapproaches to determine the magnetic anisotropy, that is, electrical measurements and magneto-optical microscopy.

A strong spin-orbit interaction is fundamental for numerous physical phenomena and leads to spin-dependent scattering processes in ferromagnets, i.e., anisotropy in the electrical transport. This anisotropy reveals itself in a transverse magnetothermopower, or PNE, where a transverse voltage is generated that depends on the mutual orientation of the in-plane magnetization and the applied temperature gradient [1,13]. The PNE is strongly dependent on the magnetic anisotropy (uniaxial and/or cubic) if present in the system, as the measured transverse voltage is sensitive to the switching of the magnetization vector between easy axes upon sweeping of the applied magnetic field. It should be mentioned that the PNE is not exclusively a feature of diluted semiconducting ferromagnets such as GaMnAs but also is observed in permalloy [14] and nickel thin films with in-plane thermal gradients [15], i.e., under experimental conditions of the so-called transversal SSE (TSSE).

Initially, the TSSE, sketched in Fig. 1(b), was reported by Uchida *et al.* [4] and Jaworski *et al.* [3]. In the so-called transverse configuration [Fig. 1(b)], the SSE is measured as a result of spin current injection from the ferromagnet (permalloy or GaMnAs, respectively) into deposited stripes of a nonmagnetic metal (Pt) and its subsequent conversion into a charge current via the inverse spin Hall effect [16,17]. A theoretical description of the phenomenon evolved with time and underwent a series of modifications for conducting and semiconducting systems [8,9]. Due to some difficulties in reproducing experimental results, the existence and significance of the TSSE are still under debate [11,14,15,18,19].

When out-of-plane thermal gradients are either intentionally or spuriously present in the system, one should be aware of the contribution arising from the ANE. In contrast to the ordinary Nernst voltage, which is a linear function of the applied magnetic field, the anomalous contribution is proportional to the magnetization of the sample. Being a thermal analog to the electric-current-driven anomalous Hall voltage, the voltage in the ANE appears orthogonal to both the sample magnetization and the applied thermal (electric) current. The ability of a compound to generate an ANE voltage depends on its ANE coefficient. For compounds with high values of the ANE coefficient, even small spurious out-of-plane gradients can result in measurable transverse voltages.

Among numerous interesting phenomena arising in GaMnAs thin films, the planar Hall effect (PHE) is a useful tool for investigating the magnetic properties of the sample. It has the same spin-orbital nature as the PNE, but instead of a temperature gradient, a charge current is required for its generation, which is easier to handle experimentally. Due to this fact, it is a useful tool for understanding the origin of the transverse voltages that appear in the PNE/TSSE, as their shape and amplitude strongly depend on the orientation of the magnetization vector. Magnetic anisotropy, if present in the sample, can therefore have a great impact on the registered thermoelectric effects and deserves proper consideration.

Recently Tang *et al.* [20] reported the observation of a giant PHE in GaMnAs films and related the behavior to the magnetic anisotropy of the system. It was shown to be very sensitive to the direction of the magnetization and, thus, could be used for the precise determination of the orientation of easy axes in the system. This technique was also developed by Shin [21,22] to determine the temperature dependence of the anisotropy constants in the system. A theory of magnetotransport for GaMnAs thin films of different growth orientations, as well as its experimental observation via either magnetoresistive or ferromagnetic resonance measurements, has recently been reported [23,24]. Although PHE experiments are of significant accuracy, they should be supported by other methods in order to provide a comprehensive understanding of the processes occurring during the magnetization reversal. As a complimentary approach magneto-optical Kerr microscopy can be successfully used.

While already known as an effective tool for derivation of the magnetic anisotropy in combination with SQUID measurements [25], direct wide-field Kerr microscopy was simultaneously applied with galvanomagnetic measuments in the present study. In addition, we have slightly increased the accuracy of the determination of the easy axes orientation, compared to Refs. [21] and [22], by fitting the angle difference between the applied magnetic field and the magnetization in the sample.

In this article we report on the experimental observation of transverse voltages generated in a GaMnAs/GaAs heterostructure in the PNE/TSSE configuration. We also investigate the ANE and discuss its contribution to the thermovoltages in the TSSE configuration via accidental out-of-plane temperature gradients. The parameters for superimposed cubic (K_c) and uniaxial (K_u) anisotropies of the sample have been extracted from PHE measurements, as well as from domain analysis using magneto-optical Kerr microscopy.

II. EXPERIMENTAL DETAILS

The heterostructures under study were grown by molecular beam epitaxy on a semi-insulating 300-μm-thick GaAs substrate with a (001) surface and consist of an undoped GaAs buffer layer and a 200-nm-thick magnetic (Ga,Mn)As film, on which lithographically patterned metallic Pt stripes were deposited. The manganese concentration was restricted to 4%. The long side of the $Ga_{0.96}Mn_{0.04}As$ film was oriented along the $[1\bar{1}0]$ crystallographic axis [see Fig. 1(a)]. The cubic anisotropy axes are along the [100] and [010] directions, while the uniaxial anisotropy is along $[1\bar{1}0]$. A special lithographic mask was designed for the deposition of 50-μm-wide Pt stripes, which allowed precise spacing, shaping, and alignment of the stripes. Two sets of samples with Pt thicknesses of 10 nm were prepared. Prior to the Pt deposition the sample surface was cleaned with acetone and isopropanol and treated with 0.1% HCl to remove the oxide layer.

The samples were carefully characterized, with an emphasis on the thermal and magnetic properties of the structure. Magnetization measurements (Fig. 2) were performed using a vibrating sample magnetometer (VSM) in a wide range of temperatures (7–300 K) and magnetic fields (0–500 mT). The sample was cooled in the magnetic field of 20 mT applied in-plane along the $[1\bar{1}0]$ direction. Afterwards the temperature dependence of the magnetic moment was taken during the

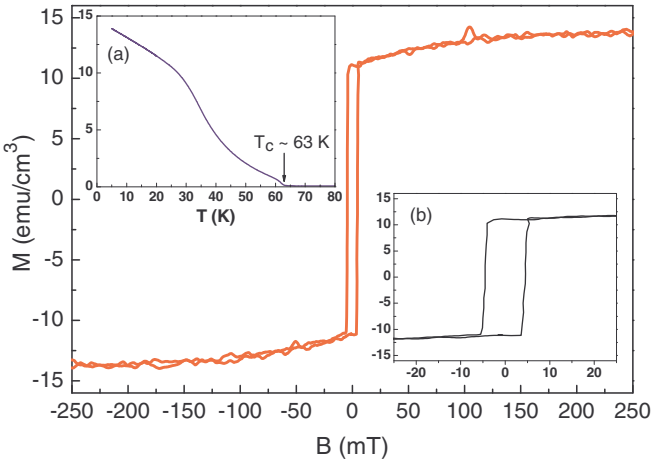

FIG. 2. (Color online) Magnetization curve measured at $T = 10$ K with the magnetic field oriented along the $[1\bar{1}0]$ direction. Inset (a): Temperature dependence of magnetization along the $[1\bar{1}0]$ direction. Inset (b): Zoom-in on the small-field region of the main curve.

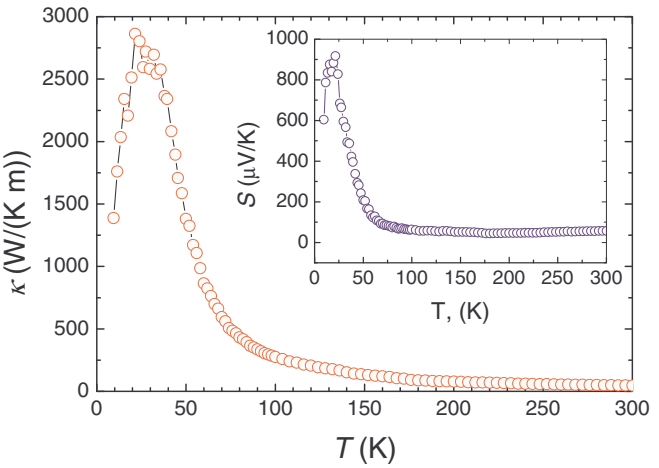

FIG. 3. (Color online) Temperature dependences of the thermal conductivity κ and thermopower S (inset) of the GaAs/GaMnAs heterostructure.

sample warming from 4 K to room temperature at applied field of 1 mT, revealing a transition from paramagnetic to ferromagnetic states at $T_c \approx 63$ K [Fig. 2, inset (a)]. Below this temperature a hysteretic behavior of the magnetization is observed in magnetic field sweeps. Coercivity increases with decreasing temperature and at 10 K a coercive force of ca. 5 mT is measured [Fig. 2, inset (b)]. The registered absolute value of the saturation magnetization is typical for the samples of similar composition [26,27]. Its upward curvature near T_c was also observed in Refs. [22] and [27] and, to our mind, is the result of inhomogeneity of the Mn distribution at such low doping concentrations.

At first glance [inset (b) in Fig. 2] saturation magnetization is reached at the field of coercivity (5 mT). However, a closer look at the magnetization curves (Fig. 2) reveals a slight variation towards the real saturation value, which is reached only at magnetic fields higher than 200 mT (at 10 K), when the magnetization entirely points in the direction of the external field.

The thermovoltage measurements were performed in two experimental setups. The first setup includes a helium-flow cryostat with a glass window for Kerr microscopy. The cryostat, in which the sample is kept under vacuum, is placed in a vector electromagnet, allowing a rotation of the magnetic field in arbitrary in-plane directions without physical reorientation of the sample. The second setup is a probe rod designed in such a way that the thermal properties of the sample are measured under vacuum conditions. The rod is inserted into a helium cryostat and surrounded by a superconducting magnet with a fixed-direction magnetic field of up to 15 T. The sample temperature can be accurately tuned in the range of 4.2–300 K via a special thermal connection between the sample and Helium. An additional radiation shield around the sample stage minimizes unwanted temperature gradients due to radiation.

Thermal conductivity and thermopower measurements were performed using a steady-state technique. The temperature gradient was created by attaching a resistive heater to one face of the sample and gluing the other face to a thermal bath. The temperature drop was measured by means of a chromel-gold thermocouple glued with GE-Vanish directly to the sample surface. The Seebeck voltage was measured with thin gold wires attached to the GaMnAs thin film with silver paste. As shown in Fig. 3, the absolute values of thermal conductivity and longitudinal thermopower rise drastically with decreasing temperature and reach maxima at 25 and 20 K, respectively. The shape of the thermal conductivity curve indicates the prevalence of phonon-phonon scattering processes in the system, while the shape of the longitudinal thermopower largely repeats that of the thermal conductivity. The high values of thermal conductivity, of the order of 2000W/(K m) in the temperature range below 50 K are related mostly to the thermal properties of the GaAs substrate, as the heat flows mainly through the thick substrate.

In order to disentangle all possible contributions of various thermoelectric effects, different experimental configurations (Conf.) were designed (Fig. 1). In Conf. A [Fig. 1(b)] an in-plane thermal gradient was applied along the long side of the sample, while the voltage was measured either on the platinum stripes or between the contacts that have been directly attached to the GaMnAs surface, transverse to the thermal gradient. The thermal gradient in the system was created either in geometry A1, where the sample was placed on top of two copper blocks, one of which served as the heater and the other as the heat sink, respectively, or in geometry A2, where the sample, a cold finger, and the heater were attached face-to-face to achieve a more homogeneous and symmetric heat flow. Heat-conducting GE-Vanish was used for gluing the heater and the thermocouple to the sample. Silver paste and gold wires (20 μm thick and 20 mm long) were used to contact the platinum stripes or GaMnAs for transverse voltage measurements. Configuration B [Fig. 1(c)] was designed for registration of the ANE. The heater was glued on the top of the sample, with a 500-μm-thick sapphire block placed in between for better heat distribution. In the last configuration C [Fig. 1(d)], the sample was fixed with Apiezon N on top of the cold finger and shielded to avoid the appearance of spurious temperature gradients in the sample. The transverse voltage

was measured while a charge current of 1 μA was passed through the sample as shown in Fig. 1(a). In this configuration a contribution from the PHE can be expected.

For all configurations in the first setup it is possible to rotate the magnetic field by 360° in the film plane, as well as to sweep the field from 0 up to ±300 mT. The in-plane rotation of the field appeared to be a useful tool for the disentanglement of thermoelectric effects arising in the presence of the magnetic field, as the generated voltage, for symmetry reasons, tends to follow different angular dependences (a cosθ dependence on the field direction for the transverse SSE and ANE and a sinθ cos θ dependence for PNE) [5,7].

For each configuration in which temperature gradients are involved, an experiment was performed as follows: At a fixed temperature below T_c, the magnetic field was swept slowly and the generated transverse voltage was measured as the difference between the voltage with the heater on and that with it off. The measurement of the voltage level after the heater was turned on or off was performed with a certain time delay, allowing transient processes to be completed, a stable temperature gradient to be established, and the environmental temperature to be adjusted to the initial temperature of the measurement (the rise of the measurement temperature is dependent on the heating power applied). The range of magnetic field sweep was varied in the different sets of experiments. At the last step of the measurement in the forward direction, the direction of the magnetic field sweep was reversed and the same set of experimental points was collected for the reverse direction. The thermally generated transverse voltage showed a hysteretic behavior on the applied magnetic field, the shape of which is analyzed and discussed in the Sec. III.

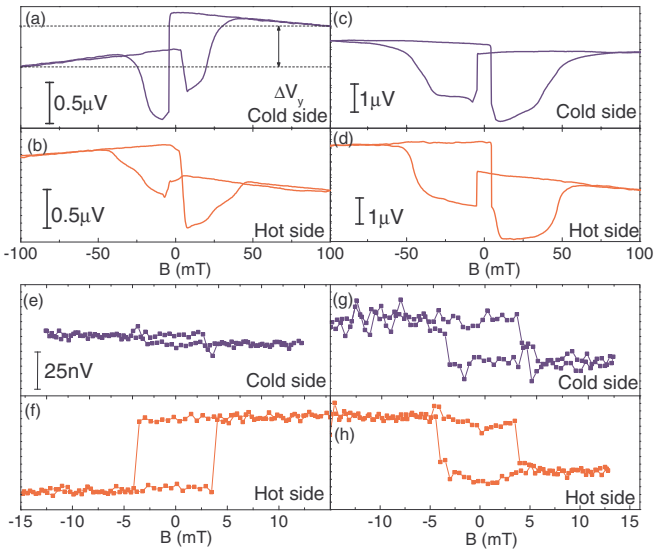

FIG. 4. (Color online) Upper panel: Voltage measurements in He flow cryostat. (a, b) Transverse voltages V_y measured at Pt stripes 1 and 4 in Conf. A1 as a function of the magnetic field swept in the direction of the temperature gradient; (c, d) Transverse voltages obtained between the pairs of contacts attached directly to the GaMnAs film and placed between Pt stripes 1 and 2 and Pt stripes 3 and 4 in Conf. A2. The heating power is 10 mW. Lower panel: Voltage measurements in the second setup (shielded probe rod) at Pt stripes. (e, f) Transverse voltages measured at Pt stripes 1 and 4 in Conf. A1 as a function of the magnetic field swept in the direction of the temperature gradient; (g, h) transverse voltages measured at Pt stripes 1 and 4 in Conf. A2. The heating power is 0.4 mW.

III. RESULTS AND DISCUSSION

A. Configuration A or SSE measurements

In our first experiments on the GaMnAs heterestructure the sample was positioned on top of the two copper blocks as shown in Fig. 1(b), Conf. A1. The temperatures of the two blocks were stabilized at 7 and 17 K, respectively, implying some in-plane temperature gradient along the [1$\bar{1}$0] direction. Such a large difference in temperatures of the copper blocks, however, does not necessarily lead to a large temperature gradient along the sample. Due to the significantly higher thermal conductivity of GaMnAs [order of 1000 W/(K m) at 10 K] compared to that of the GE-Varnish glue [order of 0.1 W/(K m) at 10 K] used to attach the sample to the measurement setup, the temperature drop occurs mostly at the glue, while the temperature drop along the sample itself is only about hundreds of millikelvins. The magnetic field was swept in the range of ±100 mT along the direction coinciding with the temperature gradient ∇T_x ($\varphi_H = 0°$).

Figures 4(a) and 4(b) show the field dependences of the transverse voltage measured on the platinum stripes on the hot and cold sides of the sample (stripes 1 and 4) in the first setup with the helium-flow cryostat. In the curves one can distinguish the parts that are symmetric and asymmetric with respect to the negative and positive field directions. While the symmetrical contribution is clearly attributed to the PNE signal [1], the asymmetric part could be an indication of the SSE as it exhibits a sign reversal between the hot and the cold ends, which is typical for the SSE [3]. Remarkably, directly contacting the GaMnAs thin film (i.e., excluding a contribution from the platinum patches or stripes) had no impact on the shape of the registered curves: both symmetric and asymmetric contributions were still present, including the sign reversal between the cold and the hot ends. This observation indicates that the signals registered in both cases originate from effects that must arise in the ferromagnetic thin film of GaMnAs itself rather than at the GaMnAs/Pt interface.

Moreover, the sign reversal between the cold and the hot ends registered in Figs. 4(a) and 4(b) vanishes when the experimental configuration A1 is modified to Conf. A2 as sketched in Fig. 1(b). Attachment of the heater and the cold finger in a face-to-face design provides a more homogeneous and symmetric heat flow through the system, thus decreasing possible out-of-plane temperature gradients in the sample. As shown in Figs. 4(c) and 4(d), where the transverse voltage was measured directly on the GaMnAs thin film after positioning the sample in the face-to-face design, the amplitude of the asymmetric contribution at the cold end is lower than that at the hot end but is, nevertheless, of the same sign.

The same series of experiments was performed on the other piece from the same batch in the second setup, with better shielding and lower heating powers. Figures 4(e) and 4(f) show the field dependences of the transverse voltage measured at the Pt stripes at the hot and the cold ends of the sample (stripes 1

and 4 at the cold and hot ends) in Conf. A1 as a heating power of 0.4 mW was passed through the sample and the magnetic field was swept within the range of only ±15 mT. The signals in Figs. 4(g) and 4(h) were measured under the same conditions (at the same Pt stripes, heating powers, and field range), but in Conf. A2. It is shown that these data demonstrate a sign reversal only in Conf. A1, and not in the more symmetric Conf. A2. This result qualitatively coincides with the one obtained in the helium-flow cryostat as presented in the upper panel in Fig. 4. This behavior suggests that the origin of the observed signals could be the ANE due to occasional out-of-plane temperature gradients.

As shown later, the directions of easy axes at low temperatures are close to the [100] and [010] crystallographic axes, and in the small-field range of 0–15 mT the magnetization vector switches by only ~90° degrees between the M_2 and M_3 axes [Fig. 7(a)]. This implies that there is always a nonzero projection of the magnetization vector on the [1$\bar{1}$0] direction, having opposite signs for positive and negative magnetic fields.

B. Configuration B or ANE measurements

To clarify whether the observed signals in Fig. 4 have a contribution from the conventional ANE, we performed experiments in Conf. B [Fig. 1(c)], where the temperature gradient ∇T_z was deliberately applied across the film thickness. The temperature was set to 5 K and the voltage was measured between the two direct contacts on the GaMnAs surface along the [110] direction. Upon the application of a 100-mW heating power, the out-of-plane temperature gradient in the ferromagnetic film is estimated to be not less than $\nabla T_z = \frac{P}{\kappa \cdot A} = 5^K/_m$ [with the area A of the sapphire plate of 4×5 mm^2 and the thermal conductivity of GaAs at 10 K assumed as $\kappa = 1000$ W/(K m)]. The voltage measured along the [110] direction with the magnetic field being swept at different angles with respect to the [1$\bar{1}$0] direction is shown in Fig. 5. The observed angular dependence is typical for the conventional ANE in a ferromagnetic material and can be analytically described by [18]

$$\vec{\nabla} V_N = -\alpha \cdot \vec{m} \times \vec{\nabla} T_z, \tag{1}$$

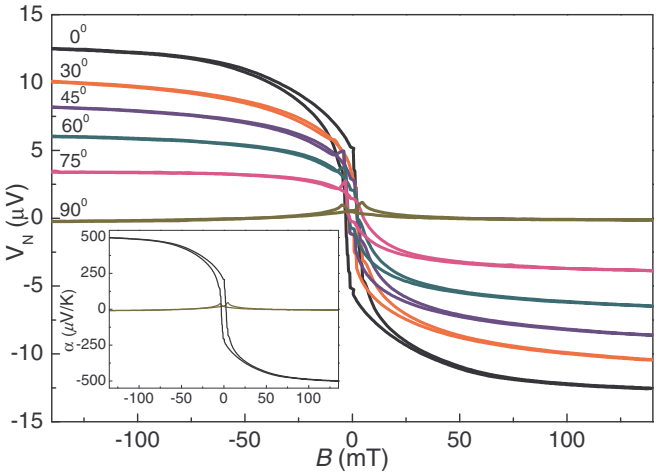

FIG. 5. (Color online) Field dependence of the voltage measured at different angles with respect to the [1$\bar{1}$0] direction in Nernst Conf. B. Inset: Field dependence of the ANE constant.

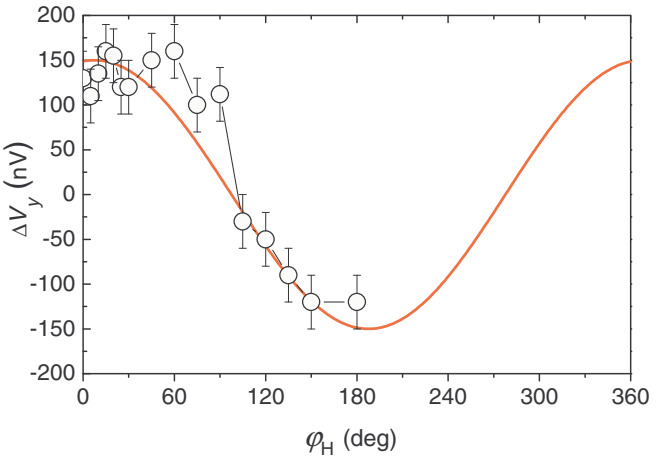

FIG. 6. (Color online) Change in the transverse voltage ΔV_y in Conf. A2 as a function of the angle between the magnetic field and the [1$\bar{1}$0] direction (open circles). Solid line represents a fit with $A \cos \varphi_H$ dependence, where A is a normalizing coefficient.

where α is the ANE coefficient and $\vec{m}$ is the unit vector of magnetization. Since the magnetization lies in-plane, the amplitude of the signal is reduced to 0 when the angle φ_H changes from 0° to 90°, thus revealing a cosine-type dependence. From these data the ANE coefficient α can be calculated as $\alpha = V_N/(l_N \cdot |\vec{\nabla} T_z|)$, where $l_N = 5$ mm is the distance between the voltage contacts. The highest value reached at $\varphi_H = 0°$ is about 500 μV/K [Fig. 5(b)], which is large in comparison to that reported by Pu *et al.* [2] for GaMnAs samples with different orientations of the easy axes with respect to the temperature gradient compared to our setup.

To get a better understanding of the origin of the asymmetric contribution in the signals presented in Fig. 4, we have examined the behavior of the transverse voltage in Conf. A2 for different in-plane orientations of the magnetic field. The voltage difference ΔV_y between the two saturated states in opposite magnetic fields ($\pm \vec{B}$) applied along the y axis is plotted in Fig. 6. One can see that the experimental points follow a cosine dependence. Such a behavior proves that the ANE, arising from spurious out-of-plane temperature gradients in the magnetic film, must be responsible for the measured signals. A slight deviation between the experimental points and the cosine dependence in Fig. 6 comes from the fact that the applied field of 100 mT is not strong enough to force the magnetization precisely along the field direction. If one considers the ANE nature of the asymmetrical contribution, then a gradient of just $|\vec{\nabla} T_z| = \frac{\Delta V_y}{\alpha l_N} = \frac{150 \text{ nV}}{500 \frac{\mu V}{K} \cdot 5 \text{ mm}} = 0.06 \frac{K}{m}$ (corresponding to a temperature drop of $\Delta T_z = 12$ nK across the 200-nm film thickness) would, in fact, be sufficient to produce $V(B)$ hysteresis loops with an amplitude of 150 nV.

C. Configuration C or the PHE and anisotropy constant

As a further step of disentanglement of the effects we have addressed the PHE effect, which has the same spin-orbital nature as the PNE. In a series of experiments we turned to Conf. C, in which the charge current was passed in the [1$\bar{1}$0] direction, while the temperature of the sample was stabilized

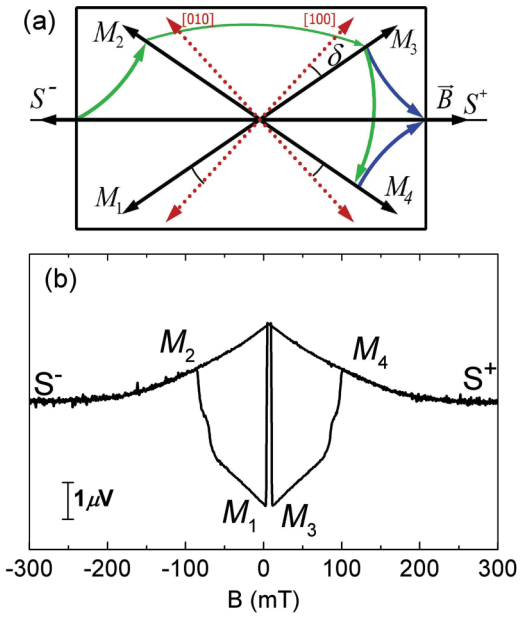

FIG. 7. (Color online) (a) Schematic of the switching process. (b) Field dependence of the Hall voltage measured in Conf. C as the magnetic field was swept in the $[1\bar{1}0]$ direction ($\varphi_H = 0°$). A charge current of 1 μA is passed in the same direction as the applied magnetic field; the temperature is 10 K.

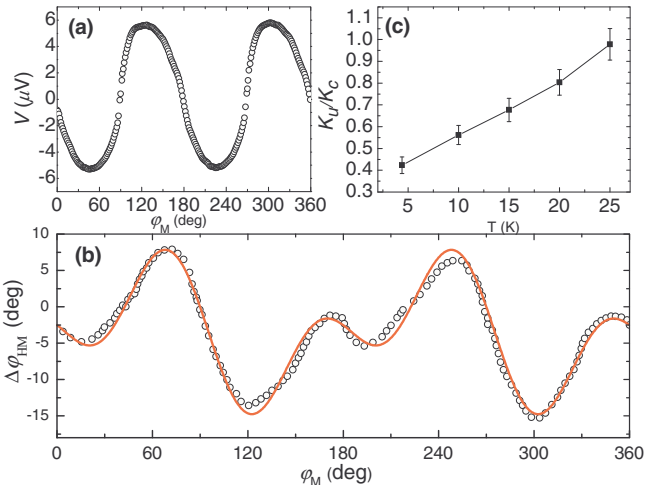

FIG. 8. (Color online) (a) Transverse voltage as a function of the angle between the applied magnetic field and the $[1\bar{1}0]$ direction. (b) The angle between the applied magnetic field and the magnetization as a function of the angle φ_M (open circles). The solid line represents a fit with Eq. (6). (c) Temperature-dependent values of the K_u/K_c ratio.

and the magnetic field was swept in-plane at different angles φ_H with respect to the $[1\bar{1}0]$ direction.

Figure 7(b) shows the transverse voltage at 10 K as a current of 1 μA was passed through the sample and the magnetic field was swept along the $[1\bar{1}0]$ direction. The curve is highly symmetric and does not contain any pronounced asymmetric contribution, in contrast to those obtained when a temperature gradient was applied. Each sweep of the magnetic field exhibits a switching between six distinct magnetic states, M_{1-4}, S^-, and S^+. This two-step ($M_2 \rightarrow M_3 \rightarrow M_4$ forward and $M_4 \rightarrow M_1 \rightarrow M_2$ backward) switching can be explained in terms of the reorientation of the magnetization in a magnetic system having four effective easy axes, originating from the competition between the cubic and the uniaxial anisotropy. States S^- and S^+ are realized when the magnetization follows a strong enough external field (higher than the saturation field). If the field is swept at different angles with respect to the $[1\bar{1}0]$ direction, the transitions $M_3 \rightarrow M_4$ and $M_1 \rightarrow M_2$ take place within the smaller field range, i.e., closer to the M_3 state.

When the magnetic field is applied in-plane and the current I is driven along the longitudinal direction of the sample, an electric field $\vec{E}$ within a single-domain ferromagnetic film with in-plane magnetization can be written as [28]

$$E_x = j\rho_\perp + j(\rho_\parallel - \rho_\perp)\cos^2\varphi_M, \tag{2}$$

$$E_x = (\rho_\parallel - \rho_\perp)\cos 2\varphi_M, \tag{3}$$

where φ_M is an angle between the magnetization direction and the density $\vec{j}$ of the current flowing along the $[1\bar{1}0]$ direction, and $\rho_\parallel$ and $\rho_\perp$ are the resistivities for the parallel and perpendicular mutual directions of the magnetization and the current, respectively.

To verify the angular dependence of the planar Hall resistance, a charge current of 1 μA and an in-plane field of a constant magnitude of 210 mT were applied and the orientation of the magnetic field was turned by 360° [Fig. 8(a)]. As the applied field is weak, the magnetization does not precisely follow the magnetic field and the experimental data slightly deviate from the expected $\cos 2\varphi_M$ dependence. From this deviation, information on the magnetic anisotropy can be derived.

The twofold switching observed in Fig. 7(b) can be explained in terms of the magnetic anisotropy of the sample: there is a superposition of the cubic anisotropy and the in-plane uniaxial anisotropy, with the easy axis of the uniaxial anisotropy being collinear with the hard axis of the cubic anisotropy. Using a Stoner-Wohlfarth model, the free energy of the in-plane magnetized sample can be written as [20,21]

$$E = K_u \sin^2\varphi_M + \frac{K_c}{4}\cos^2 2\varphi_M - M_s H\cos(\varphi_M - \varphi_H), \tag{4}$$

where K_u and K_c are the uniaxial and the cubic anisotropy constants, respectively; φ_M and φ_H are the angles of the magnetization and of the external magnetic field directions, respectively, measured from the $[1\bar{1}0]$ direction, which coincides with the charge current direction; and M_s is the saturation magnetization.

The exact positions of the energy minima $\varphi_M^{\min}$ have been determined by minimizing Eq. (4):

$$\frac{\partial E}{\partial \varphi_M} = \frac{1}{2}M_s(H_u - H_c\cos 2\varphi_M)\sin 2\varphi_M + M_s H\sin(\varphi_M - \varphi_H), \tag{5}$$

in which we have introduced the uniaxial and the cubic anisotropy fields, defined as $H_u = \frac{2K_u}{M_s}$ and $H_c = \frac{2K_c}{M_s}$. Thus, at zero field the easy axes corresponding to the four local

energy minima are oriented at $\varphi^0_{1,2} = \pm(\frac{\pi}{4} - \delta)$ and $\varphi^0_{1,2} = \pm(\frac{3\pi}{4} + \delta)$.

When the applied field is strong enough, φ_M is close to φ_H, and Eq. (5) can be approximated as

$$\Delta\varphi_{HM} = \varphi_H - \varphi_M = \frac{1}{2H}(H_u - H_c \cos 2\varphi_M) \sin 2\varphi_M. \quad (6)$$

The angles between the magnetization and the applied magnetic field as a function of the angle between the field and the current directions, obtained experimentally at 10 K and 210 mT, are shown in Fig. 8(b). Fitting this dependence with Eq. (6) and using H_c and H_u as free parameters, the uniaxial and the cubic anisotropy fields are obtained as $H_u = 50 \pm 5$ mT and $H_c = 89 \pm 7$ mT, respectively. From these values, the deviation angle δ of the easy axis orientation from the cubic anisotropy axes can be easily calculated as $\delta = 17.1^\circ$. Applying such a procedure to the angular sweeps of the magnetic field at different temperatures, we obtained the temperature-dependent anisotropy ratio K_u/K_c plotted in Fig. 8(c).

After the orientation of the easy axes is precisely determined, one can clearly understand the behavior of the field dependence of the transversal voltage, presented in Fig. 7(b). In strong negative fields (of the order of 300 mT) the magnetization follows the field and lies along the $[1\bar{1}0]$ direction [state S^- in Fig. 7(a)]. With decreasing field the magnetization slowly diverges from the S^- direction, falling on the nearest easy axis, M_2, and staying there until a small positive magnetic field is applied, when it abruptly switches to axis M_3. With further field increase the magnetization slowly switches to the M_4 orientation and, at the same time, experiences a rotation towards the field direction, until it completely follows that direction in strong positive fields. On the way back, the magnetization undergoes a similar process of switching through the $S^+ \rightarrow M_4 \rightarrow M_1 \rightarrow M_2 \rightarrow S^-$ sequence.

D. Domain studies by Kerr microscopy

The magnetic domains at different temperatures were imaged directly with a magneto-optical wide Kerr microscope. Here we present the results obtained at 7 and 20 K as being the most representative. The microscope was tuned to be sensitive to the in-plane component of the magnetization at an angle $\gamma \approx 15^\circ$ to the $[1\bar{1}0]$ direction [Fig. 10(a)]. This geometry was chosen to obtain the maximum contrast when the magnetization jumps in-plane between the M_1 and the M_2 easy axes, which is proportional to the projections of the magnetization on the direction of sensitivity (the setup is sensitive only to the component of the magnetization lying in this direction). Figure 9 (top panel) shows domain images taken at 7 K for a magnetic field applied in the direction transverse to the sensitivity direction. In the positively polarized remanent state the magnetization is aligned along the easy axis, which is (according to our earlier calculations) at about $\delta = 13^\circ$ to the [100] cubic axis. With the application of a small reversed magnetic field [Fig. 9(a)], domains with polarization along the M_2 direction are nucleated. Those domains expand with increasing magnetic field [Fig. 9(b)] until the whole sample is polarized along the M_2 easy axis [Fig. 9(c)] at 2.5 mT. With a further increase in the field, totally

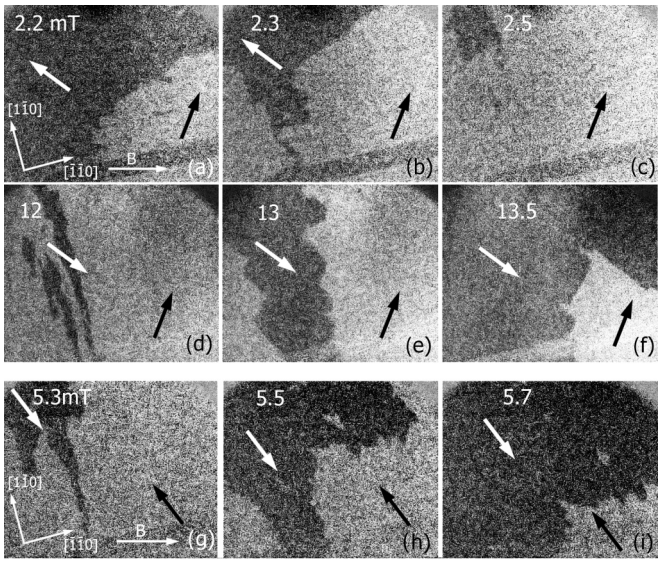

FIG. 9. Domain images taken by Kerr microscopy at 7 K (a–f) and 20 K (g–i) at the indicated fields applied at an angle $\gamma \approx 15^\circ$ to the $[1\bar{1}0]$ direction. Black arrows indicate the orientation of the magnetic moment within domain. The size of each image is 1.1 × 0.9 mm.

reversed domains with polarization along the M_4 direction are nucleated [Fig. 9(d)] and spread through the sample [Figs. 9(e) and 9(f)]. Although the domains polarized along the M_1 and M_3 axes appear black on the Kerr microscopic image, they have opposite polarizations, as the contrast was digitally enhanced and should be considered with respect to the $M_1 \rightarrow M_2$ (black → white) and $M_2 \rightarrow M_3$ (white → black) switching. This twofold switching is consistent with that observed in the voltage measurements [Fig. 7(b)] when the easy axes are at nearly 90° to each other. The switching fields correspond to those for the 75° field sweep during PHE measurements.

The evolution of the magnetic domains at 20 K is shown in Figs. 9(g)–9(i). At this temperature the deviation angle of the easy axis from the [100] direction equals $\delta = 29^\circ$,

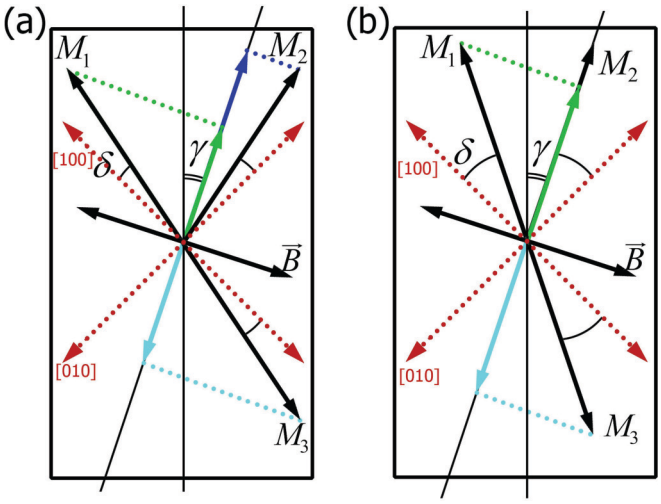

FIG. 10. (Color online) Schematic of the magnetic anisotropy of the sample at 7 K (a) and 20 K (b).

which is sufficiently larger than that at 7 K. In the negatively polarized remanent state the magnetization is aligned along the M_1 direction as at 7 K. The application of a reversed magnetic field reveals only one change of contrast with a (white → black) transition at intermediate fields, contrary to the (white → black → white) steps at small and intermediate fields at 7 K. This happens because the first switching process at small fields ($M_1 \rightarrow M_2$) cannot be seen anymore, as the difference in the magnetization projections on the direction of the Kerr sensitivity is too small to generate a contrast in the image [Fig. 10(b)]. Therefore we can resolve only the second ($M_2 \rightarrow M_3$) switching, for which the projection directions of the magnetization are opposite. The switching fields also correspond to those observed in PHE measurements at 20 K.

Specifically we have noticed a pronounced domain wall creeping as already reported in Ref. [27] and extensively studied in Refs. [25] and [29]. During creeping, the shape of the domain boundaries appears to be primarily determined by wall pinning: the boundaries between (almost) 180° domains are not zigzag folded as expected for equilibrium head-on domain walls in magnetic films [30]. For GaMnAs films the saturation magnetization ($15 \frac{\text{emu}}{\text{cm}^3} = 18.9$ mT) seems not to be high enough to enforce zigzag folding for stray-field reduction as required for regular ferromagnetic films. As a result, scalloped domain boundaries are observed.

In general, the Kerr observations confirm a strong temperature dependence of the magnetic anisotropy already revealed by PHE measurements. Similar results were obtained by using Bi-doped garnet indicator films for domain imaging [27] and by SQUID magnetometry [31]. Such an unusual behavior of a ferromagnetic material has been ascribed to the enhanced spin-orbit coupling due to the localization of holes on Mn sites with a lowering of the temperature. To clarify this, further investigations with samples of different hole concentrations or gated electrodes are required.

IV. CONCLUSION

In this paper we have performed a comprehensive investigation of thermoelectric and galvanomagnetic effects in magnetic GaAs/GaMnAs/Pt and GaAs/GaMnAs systems. Starting with the PNE/TSSE configuration, we observed field dependences of the transverse voltages consisting of symmetric and asymmetric contributions. The former is clearly attributed to the PNE arising from an in-plane temperature gradient applied along the sample, while the latter is supposed to be a manifestation of the ANE caused by spurious out-of-plane temperature gradients, as it strongly depends on the experimental geometry and follows a cosine dependence on the magnetic field typical for this effect. Using the ANE constant that was measured upon deliberately applying an out-of-plane temperature gradient, it was estimated that the rather small temperature drop of $\Delta T_z \approx 12$ nK across the 200-nm magnetic film thickness could be responsible for the appearance of spurious ANE signals, leading to the asymmetry of the thermovoltages registered in the PNE/TSSE configuration. We have also proven that the generated transverse voltage originates not from the GaMnAs/Pt interface but from the ferromagnetic film itself. This means that the TSSE, if it exists in our sample, is very likely to be negligible. Thus, all the data on spin-dependent phenomena, where temperature gradients are involved, have to be treated with great care and attention with respect to ordinary thermoelectric effects.

Direct wide-field Kerr microscopy simultaneously with galvanomagnetic measurements was applied to the investigation of the magnetic anisotropy of GaMnAs films, to the best of our knowledge, for the first time. Upon sweeping the magnetic field the development of magnetic domains was traced: at low temperatures (around 5 K) the sample exhibits a clear twofold switching of magnetization as the angle between the easy axes is nearly 90°, while at higher temperatures (above 20 K), only one-step switching was detected, indicating a collapse of the easy axes to the $[1\bar{1}0]$ direction. The same behavior of the easy axes was derived from the simultaneous transport measurements in the PHE configuration. Rotating the field in the plane of the thin film and analyzing the resulting angle dependences of the transverse voltages within a Stoner-Wohlfarth model, we obtained the anisotropy constants K_u and K_c of the GaMnAs/GaAs heterostructure. By tracing the temperature dependence of the K_u/K_c ratio, we monitored a gradual substitution of the cubic anisotropy prevailing at low temperatures with a uniaxial anisotropy with rising temperature.

Those two complementary methods of optical and transport measurements provide a precise understanding of the magnetization behavior in the sample, which is crucial for an explanation of the observed thermovoltages in PNE/TSSE and ANE configurations.

ACKNOWLEDGMENTS

We would like to acknowledge Dr. Wladimir Schoch and Dr. Wolfgang Limmer for sample growth and Sebastian T. B. Goennenwein and Sibylle Meyer for sample preparation. This work was supported by the DFG through SPP1539 (RS SCHA726/6-1 and HE 3439/9) and by the European Commission through the LOTHERM project (PITN-GA-20090238475).

[1] Y. Pu, E. Johnston-Halperin, D. D. Awschalom, and J. Shi, Phys. Rev. Lett. **97**, 036601 (2006).

[2] Y. Pu, D. Chiba, F. Matsukura, H. Ohno, and J. Shi, Phys. Rev. Lett. **101**, 117208 (2008).

[3] C. M. Jaworski, J. Yang, S. Mack, D. D. Awschalom, J. P. Heremans, and R. C. Myers, Nature Mater. **9**, 898 (2010).

[4] K. Uchida, S. Takahashi, K. Harii, J. Ieda, W. Koshibae, K. Ando, S. Maekawa, and E. Saitoh, Nature **455**, 778 (2008).

[5] A. D. Avery, M. R. Pufall, and B. L. Zink, Phys. Rev. B **86**, 184408 (2012).

[6] M. Weiler, M. Althammer, F. D. Czeschka, H. Huebl, M. S. Wagner, M. Opel, I.-M. Imort, G. Reiss, A. Thomas, R. Gross, and S. T. B. Goennenwein, Phys. Rev. Lett. **108**, 106602 (2012).

[7] D. Meier, T. Kuschel, L. Shen, A. Gupta, T. Kikkawa, K. Uchida, E. Saitoh, J.-M. Schmalhorst, and G. Reiss, Phys. Rev. B **87**, 054421 (2013).
[8] J. Xiao, G. E. W. Bauer, K.-c. Uchida, E. Saitoh, and S. Maekawa, Phys. Rev. B **81**, 214418 (2010).
[9] H. Adachi, K. Uchida, E. Saitoh, and S. Maekawa, Rep. Prog. Phys. **76**, 036501 (2013).
[10] K. Uchida, J. Xiao, H. Adachi, J. Ohe, S. Takahashi, J. Ieda, T. Ota, Y. Kajiwara, H. Umezawa, H. Kawai, G. E. W. Bauer, S. Maekawa, and E. Saitoh, Nature Mater. **9**, 894 (2010).
[11] S. Y. Huang, X. Fan, D. Qu, Y. P. Chen, W. G. Wang, J. Wu, T. Y. Chen, J. Q. Xiao, and C. L. Chien, Phys. Rev. Lett. **109**, 107204 (2012).
[12] H. Nakayama, M. Althammer, Y.-T. Chen, K. Uchida, Y. Kajiwara, D. Kikuchi, T. Ohtani, S. Geprägs, M. Opel, S. Takahashi, R. Gross, G. E. W. Bauer, S. T. B. Goennenwein, and E. Saitoh, Phys. Rev. Lett. **110**, 206601 (2013).
[13] K. Y. Wang, K. W. Edmonds, R. P. Campion, L. X. Zhao, C. T. Foxon, and B. L. Gallagher, Phys. Rev. B **72**, 085201 (2005).
[14] M. Schmid, S. Srichandan, D. Meier, T. Kuschel, J.-M. Schmalhorst, M. Vogel, G. Reiss, C. Strunk, and C. H. Back, Phys. Rev. Lett. **111**, 187201 (2013).
[15] A. D. Avery, M. R. Pufall, and B. L. Zink, Phys. Rev. Lett. **109**, 196602 (2012).
[16] J. E. Hirsch, Phys. Rev. Lett. **83**, 1834 (1999).
[17] T. Kimura, Y. Otani, T. Sato, S. Takahashi, and S. Maekawa, Phys. Rev. Lett. **98**, 156601 (2007).
[18] S. Y. Huang, W. G. Wang, S. F. Lee, J. Kwo, and C. L. Chien, Phys. Rev. Lett. **107**, 216604 (2011).
[19] D. Qu, S. Y. Huang, J. Hu, R. Wu, and C. L. Chien, Phys. Rev. Lett. **110**, 067206 (2013).
[20] H. X. Tang, R. K. Kawakami, D. D. Awschalom, and M. L. Roukes, Phys. Rev. Lett. **90**, 107201 (2003).
[21] D. Shin, S. Chung, S. Lee, X. Liu, and J. Furdyna, Magnetics, IEEE Trans. **43**, 3025 (2007).
[22] D. Y. Shin, S. J. Chung, S. Lee, X. Liu, and J. K. Furdyna, Phys. Rev. B **76**, 035327 (2007).
[23] W. Limmer, M. Glunk, J. Daeubler, T. Hummel, W. Schoch, R. Sauer, C. Bihler, H. Huebl, M. S. Brandt, and S. T. B. Goennenwein, Phys. Rev. B **74**, 205205 (2006).
[24] W. Limmer, J. Daeubler, L. Dreher, M. Glunk, W. Schoch, S. Schwaiger, and R. Sauer, Phys. Rev. B **77**, 205210 (2008).
[25] J. Honolka, L. D. Herrera, R. K. Kremer, K. Kern, E. Placidi, and F. Arciprete, New J. Phys. **12**, 093022 (2010).
[26] J. K. Furdyna, X. Liu, Y. Sasaki, S. J. Potashnik, and P. Schiffer, J. Appl. Phys. **91**, 7490 (2002).
[27] U. Welp, V. K. Vlasko-Vlasov, X. Liu, J. K. Furdyna, and T. Wojtowicz, Phys. Rev. Lett. **90**, 167206 (2003).
[28] J. Pan, *Solid State Physics* (Academic Press, New York, 1975), pp. 1–96.
[29] L. Herrera Diez, R. K. Kremer, A. Enders, M. Rössle, E. Arac, J. Honolka, K. Kern, E. Placidi, and F. Arciprete, Phys. Rev. B **78**, 155310 (2008).
[30] A. Hubert and R. Schäfer, *Magnetic Domains: The Analysis of Magnetic Microstructures* (Springer, New York, 1998), p. 686.
[31] M. Sawicki, F. Matsukura, A. Idziaszek, T. Dietl, G. M. Schott, C. Ruester, C. Gould, G. Karczewski, G. Schmidt, and L. W. Molenkamp, Phys. Rev. B **70**, 245325 (2004).